

1 **Combining computer vision and deep learning to enable ultra-scale**
2 **aerial phenotyping and precision agriculture: a case study of**
3 **lettuce production**

4
5 **Authors**

6 Alan Bauer^{1,2,3,+}, Alan.Bauer@earlham.ac.uk, orcid: 0000-0002-7443-1511

7 Aaron George Bostrom^{1,+}, aaron.bostrom@earlham.ac.uk, 0000-0002-7300-6038

8 Joshua Ball¹, Joshua.Ball@earlham.ac.uk, orcid: 0000-0003-4840-3768

9 Christopher Applegate¹, Christopher.Applegate@earlham.ac.uk

10 Tao Cheng⁴, tcheng@njau.edu.cn, orcid: 0000-0002-4184-0730

11 Stephen Laycock³, S.Laycock@uea.ac.uk, orcid: 0000-0002-7724-1369

12 Sergio Moreno Rojas⁵, sergio.morenorojas@GS-Growers.com

13 Jacob Kirwan^{5,*}, Jacob.Kirwan@GS-Growers.com

14 Ji Zhou^{1,2,3,*}, Ji.Zhou@njau.edu.cn, Ji.Zhou@earlham.ac.uk, orcid: 0000-0002-5752-5524

15

16 ¹Earlham Institute, Norwich Research Park, Norwich, NR4 7UZ, UK

17 ²Plant Phenomics Research Center, China-UK Plant Phenomics Research Centre, Nanjing Agricultural
18 University, Nanjing 210095, Jiangsu, China

19 ³School of Computing Sciences, University of East Anglia, Norwich Research Park, Norwich, NR4 7TJ

20 ⁴National Engineering and Technology Center for Information Agriculture, MARA Key Laboratory for
21 Crop System Analysis and Decision Making, Jiangsu Key Laboratory for Information Agriculture,
22 Nanjing Agricultural University, Nanjing 210095, Jiangsu, China

23 ⁵G's Growers Limited, Ely, Cambridgeshire, CB7 5TZ

24

25 ⁺Joint first author ^{*}Corresponding author

26

27 **Corresponding authors**

28 Ji.Zhou@njau.edu.cn and Ji.Zhou@earlham.ac.uk; Jacob.Kirwan@GS-Fresh.com

29

30 Abstract

31 Aerial imagery is regularly used by crop researchers, growers and farmers to monitor crops during the
32 growing season. To extract meaningful phenotypic information from large-scale aerial images collected
33 from the field, high-throughput phenotypic analysis solutions are required, which not only produce
34 high-quality measures of key crop traits, but also support professionals to make prompt and reliable
35 crop management decisions. Here, we report AirSurf, an automated and open-source analytic platform
36 that combines modern computer vision, up-to-date machine learning, and modular software engineering
37 in order to measure yield-related phenotypes from ultra-large aerial imagery. To quantify millions of
38 in-field lettuces acquired by fixed-wing light aircrafts equipped with a normalized difference vegetation
39 index (NDVI) sensors, we customised AirSurf by embedding a deep-learning classifier trained with
40 over 100,000 labelled lettuce signals. The tailored platform, *AirSurf-Lettuce*, is capable of scoring and
41 categorising iceberg lettuces with high accuracy (>98%). Furthermore, novel analysis functions have
42 been developed to map lettuce size distribution across the field, based on which associated global
43 positioning system (GPS) tagged harvest regions have been identified to enable growers and farmers to
44 conduct ultra-scale aerial phenotyping as well as precision agricultural practises to improve actual yield
45 and crop marketability before the harvest.

46

47 Keywords

48 Lettuce; ultra-scale field phenotyping; deep learning; image analysis; precision agriculture; AirSurf

49

50 Introduction

51 As an important source of vitamins, minerals, and trace elements, leaf vegetables play crucial roles in
52 human nutrition¹. Lettuce (*Lactuca sativa* L.), one of the most popular staple vegetable foods, has a
53 wide range of tastes and textures cultivated for diverse customer needs². Recent research also indicates
54 that lettuce consumption has positive effects on the reduction of cardiovascular disease and chronic
55 conditions due to its rich nutrients such as vitamin A, *Beta-carotene*, folate, and iron content³. While
56 lettuce is an important and nutritional crop, fluctuating environments can increase the fragility of its
57 production⁴. For example, the bad weather in Spain in early 2017 has led to retail prices of lettuce
58 products nearly tripled in UK supermarkets⁵. Severe weather not only causes supply shortage, but also
59 affects crop quality. According to previous studies on lettuce growth and development^{6,7}, young plants
60 at newly planted phase (i.e. from cotyledons unfolded to three true leaves stage) require cool and damp
61 weather after the transplantation from the greenhouse to the field, whereas lettuce leaves can rapidly
62 become bitter and inedible if the growth is accelerated by high ambient temperature at the head maturity
63 phase (i.e. the stage before flowering). Because of the dynamic nature of lettuce production, the actual
64 yield of lettuces in commercial operations is only around 70-80% of the planted quantity⁸. Hence, to
65 ensure the consistency of supply and quality, it is important for growers and farmers to closely monitor
66 their crops during key growth stages, so that prompt and reliable crop management decisions can be
67 made under changeable agricultural conditions⁹.

68 Aerial field phenotyping has become a popular approach for monitoring crops in recent years. Because
69 it can acquire a large number of crop imagery in field experiments using visible, thermal, and multi-
70 spectrum sensors, it has been widely applied to breeding, farming and crop research¹⁰. To ensure high-
71 quality aerial image acquisition, the flight route and altitude need to be pre-determined together with
72 the selection of appropriate imaging sensors¹¹. For example, for physiological traits such as vegetative
73 greenness and canopy structure, a high-definition RGB camera is sufficient; however, many vegetation
74 indices rely on multi- and hyper-spectral imaging sensors to assess important traits such as biomass,
75 stress level, and yield potential¹². Recently, with the development of image stitching algorithms and
76 orthomosaic generation methods, very detailed crop images can be collected by unmanned aerial

77 vehicles (UAVs) and fixed-wing light aircrafts, which enables high-quality field phenotyping and high-
78 throughput phenotypic analysis¹³.

79 To extract meaningful phenotypic information from large-scale image datasets, a variety of computer
80 vision¹⁴, machine learning (ML), and deep learning (DL) approaches¹⁵ have been utilised. In recent
81 years, much attention has been paid to ML/DL techniques, based on which computational algorithms
82 and models were built to accomplish tasks such as vision-based feature selection, image object
83 classification, and pattern prediction¹⁶⁻¹⁸. With adequate training data, suitable learning algorithms, and
84 well-defined predictive outcomes, the integration of computer vision, ML/DL, and newly emerged
85 analytic solutions (e.g. distributed computing) could lead to a step change for plant phenomics research
86 in the near future¹⁹.

87 In this article, we present a new analytic platform called AirSurf developed for ultra-scale aerial
88 phenotyping and yield-related phenotypic analysis. The software platform is open-source and combines
89 normalized difference vegetation index (NDVI) aerial imagery for data collection, computer vision for
90 image processing, deep learning (i.e. convolutional neural networks, CNNs) for crop counting, and
91 supervised machine learning for quality assessment. AirSurf was customised for commercial lettuce
92 production so that it could be used to analyse millions of lettuces across the field. We call the tailored
93 software platform “AirSurf-Lettuce” (AirSurf-L), which embeds a CNN model trained with over
94 100,000 labelled lettuce signals to measure lettuce heads and their plantation layouts using ultra-large
95 NDVI images. After scoring lettuce, unsupervised ML algorithms were used to classify lettuce heads
96 into three size categories (i.e. small, medium and large) to assess lettuce quality. To connect phenotypic
97 analysis with marketability and crop management decisions, a novel function has been developed in
98 AirSurf-L to associate global positioning system (GPS) coordinates in a given field with lettuce size
99 distribution, based on which efficient harvesting strategies could be formed to increase marketable
100 yield. .

101

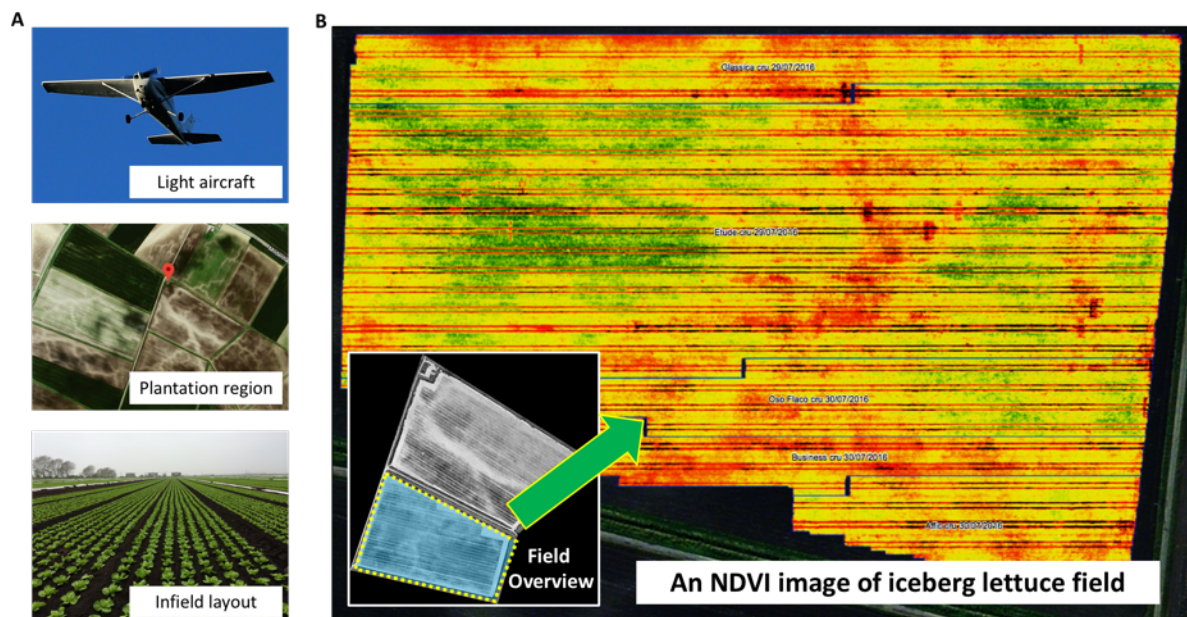
102 **Materials and methods**

103 *NDVI aerial imaging and experimental fields*

104 NDVI correlates well with leaf area index and biomass²⁰ and hence was chosen for yield-related field
105 phenotyping. The imaging sensor used is an industrial standard camera as previously described²¹. The
106 aerial imaging was carried out by a 'Sky Arrow' light aircraft, the lightest weight class (Very Light
107 Aircraft, VLA) of any commercial aircraft, which let the pilot to fly with very little fuel, less than an
108 average farm vehicle. Using VLA at 1000 feet (around 305 metres) in the sky, vast areas can be covered
109 at a flight speed of 180-200 km/hour, during which the NDVI sensor can gather ultra-scale crop imagery
110 to cover four or five fields in a single flight.

111 The ultra-large aerial NDVI imagery was acquired routinely (i.e. four-five times per season) by G's
112 Growers, the second largest vegetable grower in the UK. The flying route and the imaging protocol
113 were designed to facilitate cross-site crop assessment and yield prediction (Fig. 1A). In this study, we
114 used a series of collected ultra-large NDVI images (1.5-2GB per image) at 3cm ground sample distance
115 (GSD) spatial resolution, for iceberg lettuces at H1 and H2 stages (i.e. moderate compact and crushable
116 head), before lettuce leaves were largely overlapped. Experimental fields in the study were all located
117 near Ely, Cambridgeshire UK, ranging from 10 to 20 hectares, with between 800,000 and 1.6 million
118 lettuce heads in a single field. One field (Field A) planted with around 1 million lettuce heads was used
119 to explain the analysis workflow and associated algorithms of AirSurf-L in the following sections (Fig.
120 1B). A high-level manual yield counting was conducted by G's growers' field specialists during the
121 harvest, which was used to verify and improve the platform. Lettuces in subsections randomly selected
122 from Field A were scored manually by laboratory technicians and then used as training datasets for the
123 deep learning model.

124



125

126 **Figure 1: Ultra-scale NDVI aerial imaging accomplished routinely through a fixed-wing light aircraft**
 127 **operated by G's Growers.**

128 (A) The flying route and aerial imaging were designed to facilitate cross-site crop layout assessment and yield
 129 prediction. (B) A series of ultra-large NDVI images at 3cm GSD spatial resolution were acquired to record 0.8-
 130 1.6 million lettuce heads per field, at H1 and H2 stages.

131

132 *Data construction for training and testing*

133 To generate sound datasets for ML-based image analysis, we randomly selected 60 patches of the
 134 field of varying sizes, each containing between 300 and 1,000 lettuce heads. We then manually labelled
 135 each lettuce in the selected patches with a red dot ([Supplementary Fig. 1](#)). Each labelled lettuce, i.e. a
 136 red dot, is identified by a 20x20 pixel bounding box representing a single lettuce head. We then used
 137 these bounding boxes, as well as images that did not correspond to a lettuce head, to train a CNN
 138 classifier to recognise and separate potential lettuces in the plantation field. The pixels contained within
 139 a bounding box were also used for defining lettuce size. A training dataset with over 100,000 20x20
 140 pixel labelled bounding boxes has been created, amongst which 50% are lettuces and the remaining are
 141 background signals such as soil, edges of the field, and other non-lettuce objects. Following a standard
 142 CNN segmentation approach²², we designed a non-overlapping sliding window function to go through
 143 the whole field to separate foreground and background signals, splitting lettuce and non-lettuce objects.

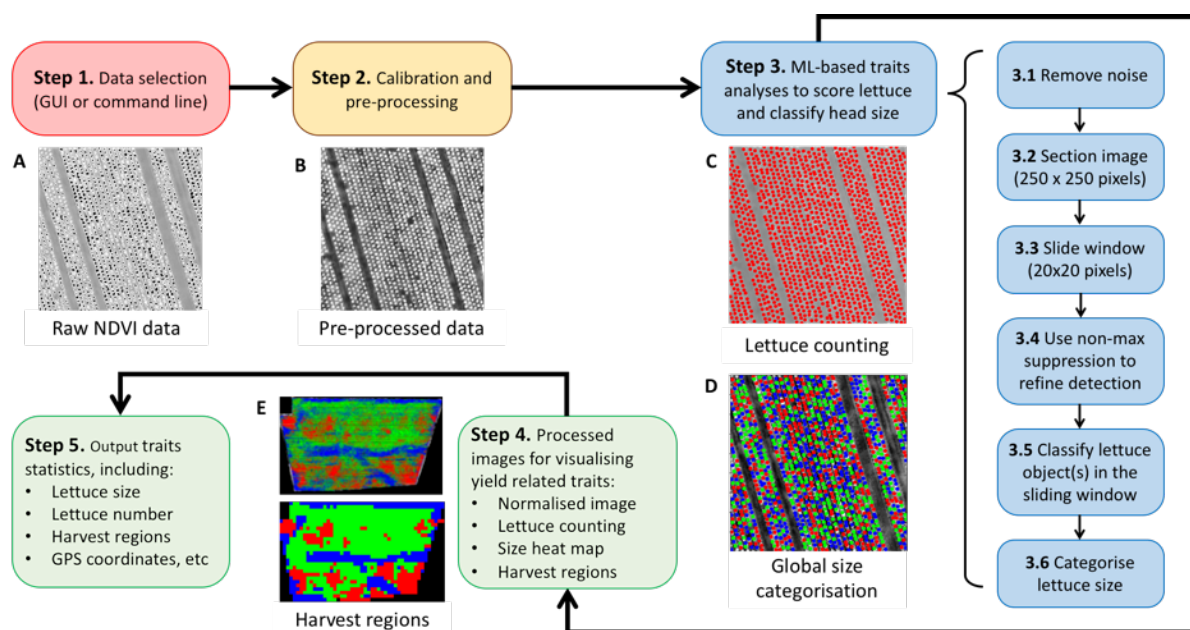
144 Training and testing datasets are equally balanced. Validation sets are used alongside training sets to
 145 verify the performance of the model, which also prevent overfitting in model training and allow us to
 146 fine-tune hyperparameters of different learning layers²³.

147

148 *The analysis workflow of AirSurf-Lettuce*

149 The analysis of yield-related phenotypes was based on NDVI signals of iceberg lettuces across the
 150 field. [Figure 2](#) shows a high-level analysis workflow of AirSurf-L, which consists of five steps: data
 151 input, image calibration and pre-processing, ML-based traits analyses, results visualisation, and
 152 quantifications of yield-related phenotypes. *Step 1* accepts raw NDVI images as gray-level imagery
 153 datasets. As pixels with extremely high NDVI signals usually have overflowed intensity values (i.e.
 154 black pixels in [Fig. 2A](#)), a pre-processing step (*Step 2*) is designed to calibrate raw NDVI images, so
 155 that intensity distribution can be normalised to correct overflowing pixels. At this step, an algorithm
 156 called contrast limited adaptive histogram equalization (CLAHE)²⁴ is applied to increase the contrast
 157 between the foreground (i.e. lettuces) and background (e.g. soils) in a given NDVI image ([Fig. 2B](#)).
 158 [Supplementary File S1](#) provides pseudo code and explanations of the image calibration and pre-
 159 processing step to ensure high-quality inputs of the learning model.

160



161

162 **Figure 2: A high-level analysis workflow of AirSurf-Lettuce.**

163 (A) Step 1 accepts raw NDVI images as input imagery data (pixels with extremely high NDVI signals are
164 overflowed). (B) Step 2 pre-processes the raw NDVI images to calibrate intensity distribution and correct
165 overflowing pixels. (C&D) Step 3 carries out ML-based traits analyses to quantify lettuce number and classify
166 head size in a given NDVI image. (E) Steps 4&5 visualise and export statistics of the traits analyses detection,
167 including yield-related phenotypes such as lettuce counting, size distribution, and harvest regions, and associated
168 GPS coordinates.

169

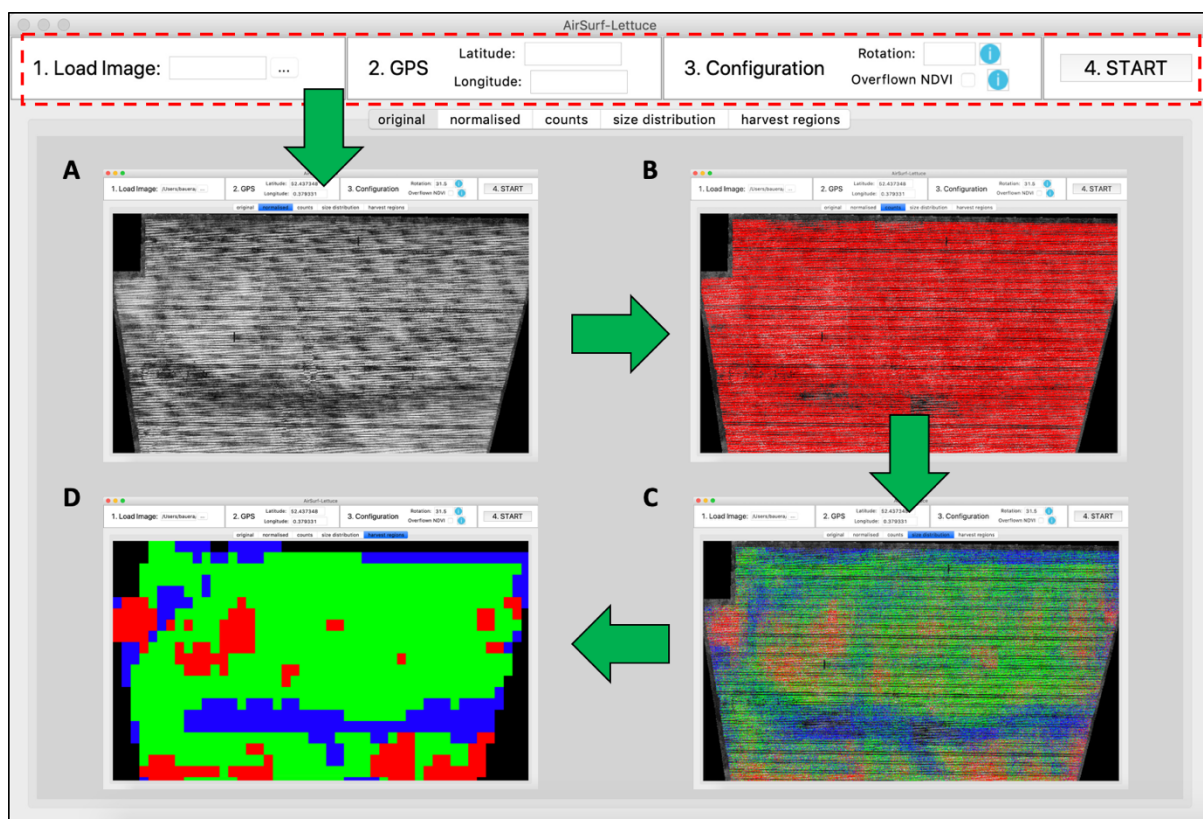
170 *Step 3* carries out ML-based traits analyses that quantify lettuce number (Fig. 2C), as well as classify
171 head size (Fig. 2D). It includes six steps: removing noise signals, partitioning a given image into
172 sections (250 x 250 pixels) for local analysis, producing a sliding window (20 x 20 pixels) to traverse
173 within a sectioned image, using non-max suppression to detect lettuces, and classifying recognised
174 lettuces into three size categories (i.e. small, medium and large). The analysis result is visualised in
175 *Step 4*, where lettuce counting, size distribution map, and GPS-tagged harvest regions are saved as a
176 series of processed images (Fig. 2E). At the final step (*Step 5*), statistics of yield-related traits are
177 exported to a comma-separated values (CSV) file, including lettuce counts per field, lettuce size
178 distribution, lettuce number and size measures within GPS grids, harvest regions, and associated GPS
179 coordinates (Supplementary File S2). To enable users to carry out the above analysis workflow easily,
180 a graphical user interface (GUI) software application has been developed.

181

182 *AirSurf-Lettuce GUI*

183 The GUI of AirSurf-L (Fig. 3) was developed using the native python GUI package, Tkinter²⁵, which
184 allows the software application to be executed on different operating systems such as Windows and
185 Mac OS (note: we only provided a packaged .exe executable file on the GitHub). Following the systems
186 design described previously²⁶, the GUI uses an easy-to-follow approach to implement the phenotypic
187 analysis workflow. The GUI window is divided into two parts: input section and display section. In the
188 input section (dash rectangle coloured red in Fig. 3), a user needs to firstly load an NDVI image, which
189 will be displayed instantaneously in the display section (dash rectangle coloured green), the *original*

190 tab. Secondly, the user needs to enter GPS coordinates of the field (i.e. the top left corner of the input
 191 image, which can be retrieved from the metadata or Google Maps). Thirdly, the user is required to
 192 define the rotation value of the input image in degrees in comparison with the north geographical
 193 direction, so that GPS calculation can be standardised. Then, the user needs to tell the software whether
 194 the input image contains overflowed NDVI signals; if so, an extra calibration process will be triggered
 195 (Fig. 2, *Step 2*). Finally, after entering a small number of inputs, the user can click the Start button to
 196 initiate the analysis workflow.



197

198 **Figure 3: Two sections designed in the AirSurf-Lettuce GUI.**

199 (A) A processed image after pre-processing and calibration (in the normalised tab). (B) A processed image after
 200 lettuce counting (in the counts tab). (C) A processed image after lettuce size categorisation (in the size distribution
 201 tab). (D) A processed image after identifying harvest regions and commuting GPS coordinates (in the harvest
 202 regions tab).

203

204 The GUI software follows each step in the workflow to conduct the automated phenotypic analysis.

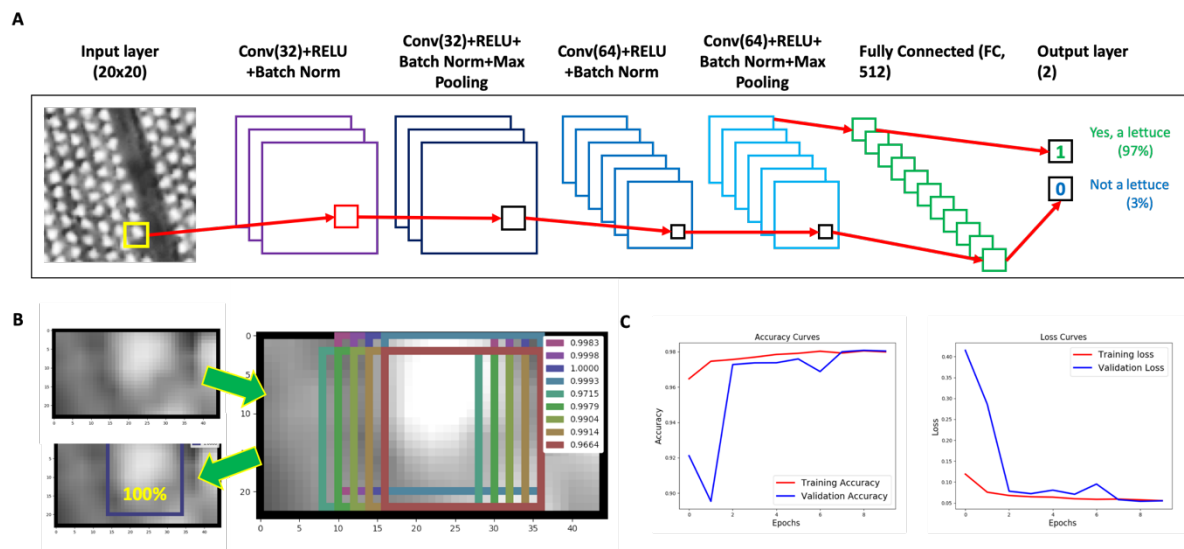
205 When a step is accomplished, an associated processed image will be displayed in the display section,

206 showing the result of the intermediate result of the analysis. Four processed images will be presented:
207 a pre-processed and calibrated image (Fig. 3A, in the *normalised* tab), an image after lettuce scoring
208 (Fig. 3B, in the *counts* tab), an image after size categorisation (Fig. 3C, in the *size distribution* tab), and
209 a processed image after identifying harvest regions and their associated GPS coordinates (Fig. 3D, in
210 the *harvest regions* tab). All processed images are saved in a result folder, along with a CSV file that
211 contains trait analysis results ([Supplementary File S2](#)).

212

213 *Neural network architecture*

214 Similar to AlexNet²⁷, a CNN-based learning architecture was established using the labelled datasets.
215 [Figure 4A](#) demonstrates the architecture of the CNN model, including (1) a convolutional (Conv2D)
216 layer with 32 filters and a 3x3 kernel, with a rectified linear unit (ReLU) as the activation function, and
217 batch normalisation to accelerate the learning process to enable higher learning rates²⁸; (2) the same
218 block is then repeated together with a max pooling layer to down-sample input using a 2x2 kernel based
219 on the assumption that useful input features could be contained in sub-regions; (3) after that, a second
220 convolutional block is constructed, consisting of a Conv2D layer with 64 filters, a 3x3 kernel, a ReLU
221 activation, and batch normalisation; (4) finally, this block is repeated, followed by another max pooling
222 layer (with a 2x2 kernel) to complete the learning procedure. After the convolutional layers, layers are
223 connected to a fully connected layer of size 512, which is followed by a dropout layer with a 50%
224 chance. To complete the learning architecture, a binary output generates the probability of whether a
225 given bounding box (20x20 pixels) contains a lettuce signal. If the probability equals or is close to 1.0
226 (i.e. 100%), it indicates that it is highly likely that the bounding box contains a complete lettuce head
227 ([Fig. 4B](#)). The above architecture is commonly applied to vision-based object detection problems²⁹.
228 The training and validation accuracy and loss curves are reported in [Figure 4C](#), showing that the model
229 converges in only 10 epochs. More importantly, to avoid overfitting, the stopping criterion was designed
230 to guarantee the validation accuracy is higher than the training accuracy, ensuring the generalisation of
231 the learning model. To avoid the overfitting issue of our model, the labelled data was also divided
232 equally into train and validation sets, when training the model.



233

234 **Figure 4: A CNN-based learning architecture established for lettuce counting.**

235 (A) The architecture of the trained CNN model, which generates a binary output representing the probability of
 236 whether a yellow bounding box contains a lettuce signal. (B) If the probability is close to 1.0, it indicates that it
 237 is highly likely that the bounding box encloses a lettuce. (C) The training and validation accuracy and loss curves
 238 of the model.

239

240 The architecture is shallower than AlexNet and other modern deep learning architectures for a number
 241 of reasons: (1) the size of our dataset is relatively small for establishing very deep learning networks;
 242 (2) our target is a binary classification problem (i.e. whether or not a given bounding box contains a
 243 whole lettuce head), opposing to ImageNet classification tasks; (3) larger and deeper neural networks
 244 require more time to train, which can be slower to execute and not feasible for prompt decision making
 245 requirements in precision agriculture.

246

247 *Size categorisation algorithm*

248 After AirSurf-L identifies bounding boxes containing lettuce heads, we employed an unsupervised
 249 ML approach to categorise lettuce into three sizes: small, medium and large. The algorithm can be
 250 easily changed to classify more size categories, if required. Pixels in the bounding box region are
 251 extracted and then NDVI values of all the pixels are put into bins. The histogram included 10 bins that
 252 spread across the NDVI value range (0-255). We included two important aspects when categorising

253 lettuce sizes: (1) lower NDVI surrounding values do not determine the lettuce size; (2) higher NDVI
254 values are more important in indicating the size. As such, a geometric pattern of NDVI values for each
255 bin was created, i.e. 64, 128, 160, 192, 208, 224, 232, 240, 244, 248, 250, 252, 253, and 254. With these
256 cut-off values, most of the background pixels were captured in the first two bins, along with increasing
257 weight when the values approach 255.

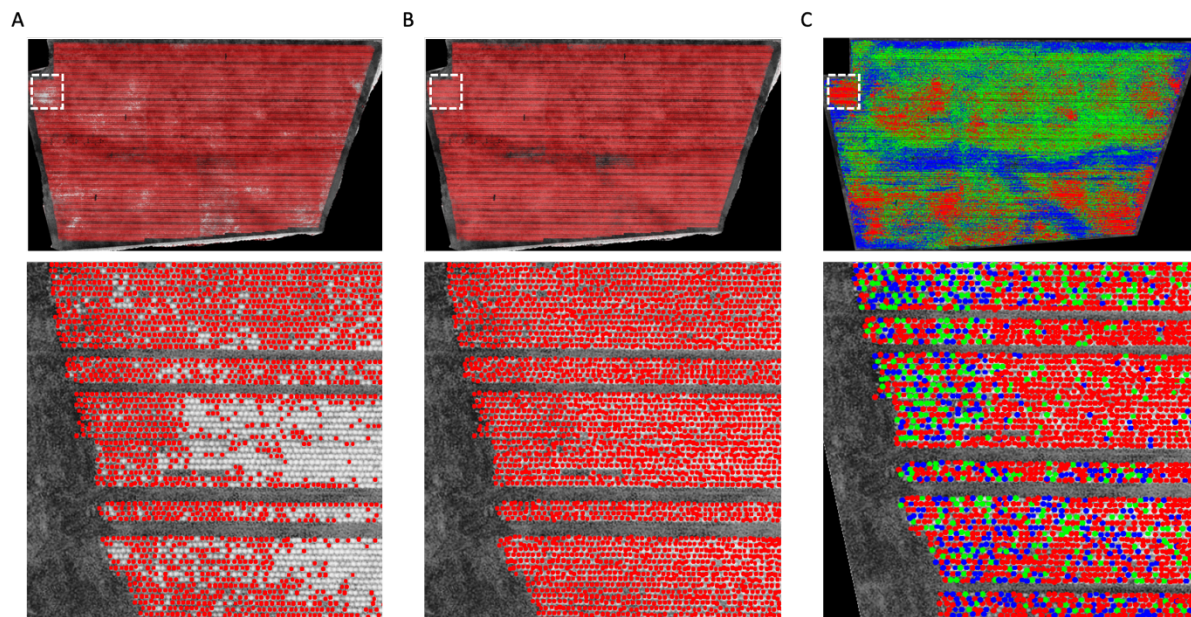
258 Having transformed the pixel regions into a series of bins, we were able to compare regions and
259 cluster them into three size groups using k-means clustering with k set to three. Then, clustering results
260 are sorted through calculating the dot product between the weight vector and the cluster count vector
261 (based on bins). These sorted values determine which clustering result corresponds to which size, which
262 are then applied to each lettuce detected in the field. Three colours are used to indicate size categories:
263 blue for small, green for medium, and red for large (Fig. 3C).

264

265 **Results**

266 *Counting lettuces with a CNN classifier*

267 After a CNN classifier was trained and the phenotypic analysis algorithms were implemented in the
268 AirSurf-L, we used the software to recognise and classify lettuce signals in ultra-large NDVI images.
269 Initially, a broad range of sizes and orientations of lettuces with varying intensities were captured;
270 however, the software failed to recognise lettuces in very bright regions and overly count lettuces in
271 very dark regions (Fig. 5A), e.g. around 50,000 lettuces were wrongly detected in a one-million-head
272 field (5% counting error). We found that this problem was caused by the trained CNN classifier, because
273 a lettuce head is extremely tiny in an orthomosaic image (e.g. 11,330x6,600 pixels for a 7-hectare field
274 when GSD is 3cm, which contains over half million lettuces) under extreme lighting conditions. To
275 resolve this issue, we have designed a two-step solution: (1) sectioning the whole image into many
276 250x250 pixels sub-images, and (2) using a fix-sized bounding-box (20x20 pixels) as a sliding window
277 (with a stepping parameter of 5 pixels to reduce the sliding calculation) to prune the detected lettuce
278 objects in each 250x250 sub-image.



279

280 **Figure 5: The improved results of the CNN model and the size classification of lettuce heads.**

281 (A) Wrongly detected lettuces in very bright regions and overly counted lettuces in very dark regions, in a one-
282 million-head field. (B) Enhanced training datasets to retrain the model using the online-learning approach, which
283 led to much better detection results. (C) A predefined colour code (small is coloured blue, medium is coloured
284 red, and large is coloured green) is assigned to each recognised lettuce head across the field.

285

286 Another reason that caused the detection is due to overlapped lettuces as overlapped lettuces could be
287 detected repeatedly by the CNN classifier in a sub-image. Hence, we employed a non-maximum
288 suppression (NMS) algorithm³⁰ to rectify the detection result. NMS uses probabilities to order the
289 detected lettuce objects. After the 20x20 sliding window is performed and many small patches have
290 been identified, the NMS algorithm computes an overlap coefficient to determine how to retain these
291 patches. As lettuces are relatively well-spaced in the field, patches (i.e. bounding boxes) enclosing a
292 complete lettuce signal are retained, whereas partially covered signals will be removed. To select the
293 best overlap parameter computed by the NMS, a gradient descent method is formulated and explained
294 in [Supplementary File S3](#).

295

296 *Improved CNN classifier and the size categorisation*

297 Besides the improved computer vision approach, we also enhanced the training datasets by manually
298 labelling an additional 500 lettuce signals within very bright or very dark regions. Then, newly labelled
299 data was inserted into the training datasets to retrain the model through the online-learning approach³¹.
300 The improved CNN model (see GitHub repository and [Supplementary File S4](#)) was tested on different
301 experimental fields again and has dramatically enhanced the detection result ([Fig. 5B](#)).

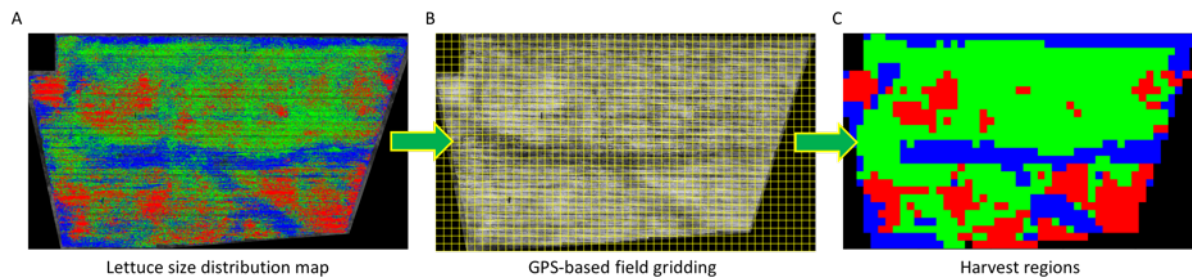
302 Identified lettuces are individually analysed to determine their associated size category. The size
303 classification is based on intensity and contrast values enclosed by the 20x20 bounding boxes, which is
304 computed using the dot product of the histogram of pixel intensities and a weighted vector towards
305 more pixel-based contrast values. The assumption of this design is that higher NDVI signals likely
306 correlate with higher vegetation indices and hence bigger lettuce heads. The categorisation result of all
307 lettuce heads is clustered into three size groups. Each lettuce is then coloured with a predefined colour
308 code (i.e. small is blue, medium is green, and large is red, see [Fig. 5C](#)).

309

310 *A GPS-tagged harvest map*

311 The final phase of the phenotypic analysis is to define harvest regions based on different sizes of
312 lettuces. Using the size distribution map ([Fig. 6A](#)), the field is firstly segmented into many small grids
313 based on the optimal GPS resolution determined by the altitude of the aerial imagery (i.e. 3cm GSD, in
314 our case) as well as the size of the harvester machinery used by the grower. After dividing the field into
315 thousands of grids ([Fig. 6B](#)), GPS coordinates of each grid are computed and each grid is then coloured
316 with the most representative size category. By combining all coloured grids, a GPS-tagged harvest map
317 is produced, representing harvest regions of the whole field ([Fig. 6C](#)). The harvest map can be used for
318 designing harvesting strategies such as guiding a harvester to collect desired sized lettuces or arranging
319 logistics based on the lettuce number and associated size counting. To facilitate precision agricultural
320 practices, a result file ([Supplementary File S2](#)) is generated by AirSurf-L at the end of the analysis,
321 containing information of each harvest grid, the associated GPS coordinates, lettuce size and number

322 counting in each grid. To satisfy different needs for dissimilar requirements, the size of GPS-based
323 harvest grids can be modified manually in the software.



324

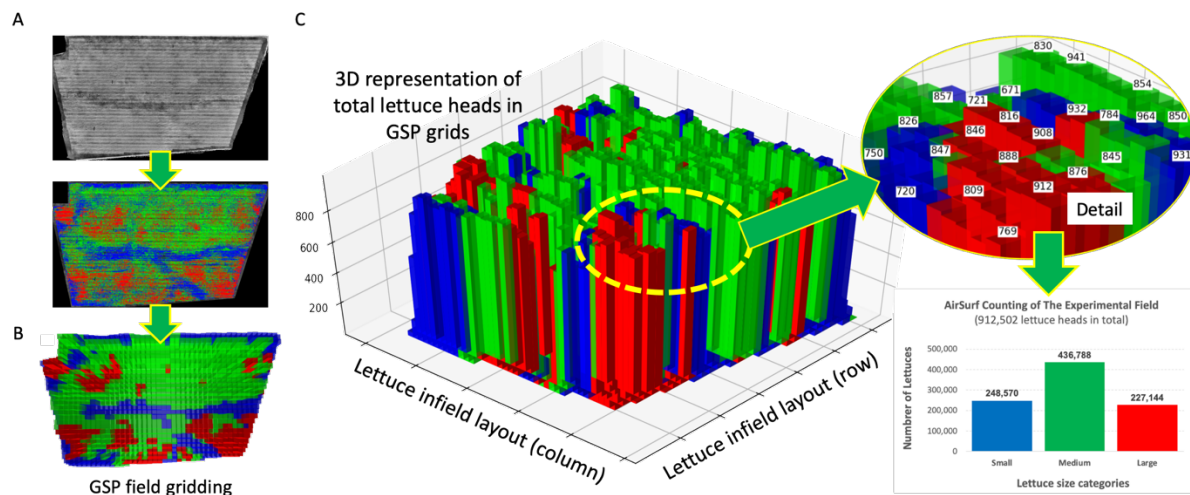
325 **Figure 6: A GPS-based harvest map based on lettuce size classification.**

326 (A) A colour-coded lettuce size distribution map (small is coloured blue, medium is coloured green, and large is
327 coloured red). (B) The field is segmented into thousands of grids based on the optimal GPS resolution and the
328 size of the harvester machinery. (C) Grids are coloured with the most representative lettuce size category across
329 the image, representing harvest regions of the whole field.

330

331 *3D visualisation for the harvesting strategy*

332 [Figure 7](#) uses Python-based 3D Matplotlib library³² to show the GPS-tagged harvest map. When
333 AirSurf-L reads an NDVI image, it computes the number of lettuce heads and associated size categories
334 on the image ([Fig. 7A](#)). Then, by combining GPS-based field grids with the representative lettuce size
335 in these grids ([Fig. 7B](#)), we produced a Python-based dynamic 3D bar chart script ([Supplementary File](#)
336 [S5](#)) to present the lettuce number using the z axis, infield layout (both columns and rows) using both x
337 and y axes, and the representative lettuce size using the predefined colours ([Fig. 7C](#)). Through the 3D
338 plot, users can zoom into any sub-region of the field to check lettuce number and representative size so
339 that a precise harvesting strategy can be planned accordingly. The overall lettuce number and size
340 counting of the experiment field can also be calculated.



341

342 **Figure 7: 3D visualisation of lettuce harvest regions.**

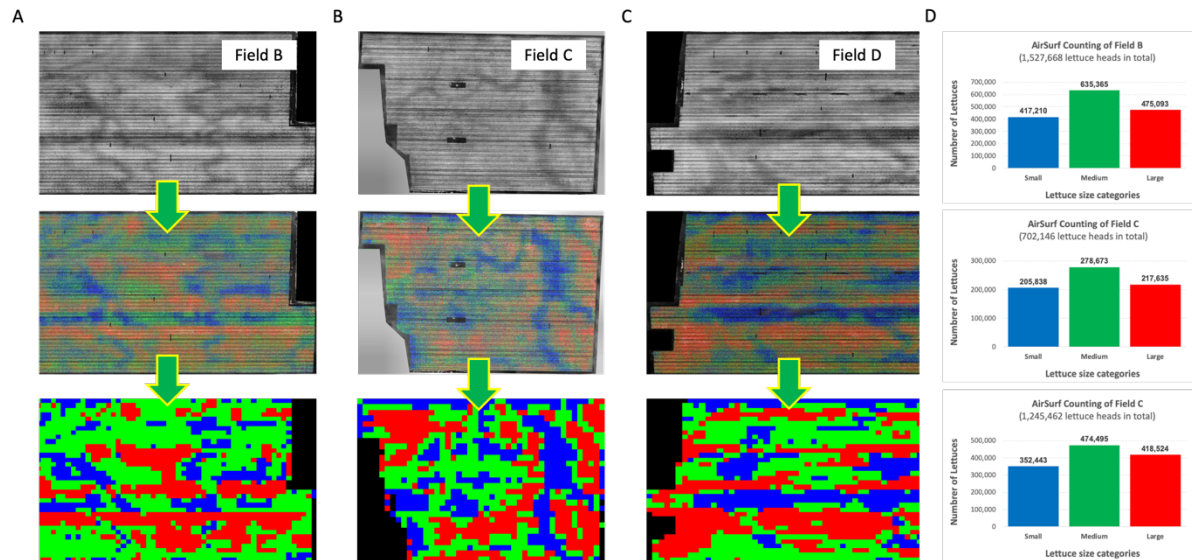
343 (A) AirSurf-L reads an NDVI image and exports a lettuce size distribution map, where small lettuce is coloured
 344 blue, medium size is coloured green, and large lettuce is coloured red. (B) 3D visualising GPS-based field grids
 345 to present representative size categories. (C) A dynamic 3D bar chart is generated to present the relationship
 346 between lettuce number, infield layout, and the representative lettuce size, along with over lettuce number and
 347 size quantification.

348

349 *Validation of AirSurf-Lettuce*

350 To verify AirSurf-L and the soundness the algorithm, we have applied the platform to count and
 351 classify lettuce heads in three unseen experimental fields in Cambridgeshire, UK (Figs. 8A-C). These
 352 fields contain between 700,000 and 1,500,000 lettuces and are located in different sites around the
 353 county. Traits such as the number of lettuces per field quantified by the platform (Fig. 8D) were
 354 compared with industrial estimates, showing a low error in lettuce counting (<5% difference). Besides
 355 the field-level comparison, we also randomly selected different sizes of subsections in an experiment
 356 field to evaluate AirSurf-L. We split these subsections into three sets (i.e. 36 small regions, 21 large
 357 regions, and 57 mixed regions), where the small regions have less than 400 lettuces, the large ones
 358 contain greater than 900 lettuces heads, and mixed regions contain a variety of lettuce heads. After that,
 359 laboratory technicians manually counted lettuce heads within these regions. The correlation between
 360 the manual and automated lettuce counting shows that, for the small regions, the difference between the
 361 human and automatic counting is approximately 2% ($R^2 = 0.978$); for the large regions, the average

362 difference is around 0.8% ($R^2 = 0.988$); and for mixed regions, the R^2 correlation is over 0.9997.
 363 [Supplementary Figure 2](#) and [Supplementary File S6](#) show the correlations between human and
 364 automatic counting for all three region groups.



365
 366 **Figure 8: Applying AirSurf-Lettuce to count and classify millions of lettuce heads in three plantation fields**
 367 **across the Cambridgeshire, UK.**

368 (A-C) AirSurf-Lettuce is applied to count and classify millions of lettuce heads (small is coloured blue, medium
 369 is coloured green, and large is coloured red), in three plantation fields in the Cambridgeshire, UK. (D) The overall
 370 quantification of Lettuce heads and size categories in three fields.

371

372 Discussion

373 Traditionally, measuring in-field crops on a large scale is very time-consuming and labour-intensive.
 374 It often requires destructive techniques, potentially error-prone manual counting, or estimates of traits
 375 that are key to yield production or crop quality³³. Recent advances in ML/DL and CV techniques have
 376 led to an explosion of plant phenomics, which has rapidly improved our abilities in mining phenotypic
 377 information from large and complicated phenotyping datasets³⁴. New data-driven analytic approaches
 378 are also changing plant phenomics – collecting big data (i.e. phenotyping) is no longer the bottleneck,
 379 instead how to extract biologically relevant information (i.e. phenotypic analysis) from big data has
 380 become the current challenge³⁵. Hence, along with the development of aerial imaging and remote
 381 sensing technologies, it has become increasingly noticeable that the integration of scalable data

382 collection, high-throughput phenotypic analysis, and yield predictive modelling are key to crop research
383 and precision agriculture³⁶.

384 AirSurf-L introduced here has addressed a specific challenge in ultra-scale aerial phenotyping and
385 precision agricultural management through combining aerial NDVI imagery, CV, ML/DL, software
386 engineering, with commercial lettuce production. The platform automates the measurement of millions
387 of lettuces across the field, which allows us to connect research-based phenotypic analysis with real-
388 world agriculture problems. As a cross-disciplinary project, we have chosen an agile R&D method,
389 because technologies and business requirements were constantly changing in the project. The results
390 generated by AirSurf-L show a strong correlation between automatic counting and specialist scoring
391 ($R^2 = 0.98$). Hence, we are confident that AirSurf-L is capable of assisting fresh vegetable growers and
392 farmers with their phenotyping needs as well as yield-related trait analysis.

393

394 *Commercial impacts*

395 Commercially, lettuce production offers an attractive economic profitability in comparison to many
396 other Agri-Food businesses³⁷. To date, lettuce businesses are worth billions of dollars and employ
397 hundreds of thousands of permanent and seasonal workers globally. European vegetable growers alone
398 produced 2.95 million tonnes of lettuce (and chicory) in 2016, a total annual value of €2.5 billion³⁸.
399 Further down the fresh produce supply chain, the planning and efficiency of many essential crop
400 production activities are largely dependent on crop maturity date and the marketability of crops (i.e. the
401 crop quality)³⁹. Marketing activities such as logistics, trading, and product marketing need to be
402 organised several weeks before the harvest; moreover, the booking and reservation of crop distribution,
403 agricultural equipment, and associated commercial plans with retailers also need to be determined
404 beforehand⁴⁰. By doing so, crop can be harvested at the right time, with maximised yield⁴¹. Our work
405 contributes directly to lettuce production for improving the actual yield of lettuces and is also capable
406 of reliably quantifying crop quality (e.g. lettuce size), both of which are key to the success of crop
407 production, marketing, and supply chain management.

408

409 *Machine learning and computer vision in plant phenomics*

410 Another aim of this work is to further ML- and CV-based software solutions in plant phenomics. High-
411 throughput plant phenotyping is a fast-growing research domain, covering many disciplines, from plant
412 breeding, cultivation, remote sensing, to computing sciences⁴². The modulated software development
413 allows us to apply different open-source learning architectures⁴³ (e.g. the TensorFlow frameworks) and
414 CV algorithms⁴⁴ (e.g. Scikit-Image libraries) to AirSurf-L. Notably, it is worth pointing out that we
415 have learned a number of lessons when applying ML/DL and CV in phenotypic analysis: (1) learning
416 algorithms could perform badly if training datasets are not well-labelled and insufficient; (2) although
417 ML/DL algorithms specialised in segmentation and classification if target objects are well-defined,
418 there is still a big gap between object recognition and traits analyses; (3) meaningful phenotypic analysis
419 not only requires sufficient biological understanding to define target traits in a logical manner, but also
420 needs bespoke algorithms to engineer features so that traits can be soundly quantified. Hence, in plant
421 phenomics research, biological questions, analytical solutions, and software implementation need to be
422 considered collectively in order to address complicated plant phenomics challenges.

423

424 *Limitations and further development of the platform*

425 Besides the convincing phenotypic analysis results presented in this article, there are still limitations
426 of the platform need to be considered: (1) AirSurf-L has been tested with top-view iceberg lettuces
427 mainly at H1 and H2 stages, which means that analysis error could increase if there are too many
428 overlaps between lettuce heads, e.g. from H3 stage onwards. (2) As AirSurf-L has only been tested with
429 NDVI imagery, it is important to add new functions to the platform to incorporate other vegetation
430 indices measurements through multi- and hyper-spectrum imaging sensors. (3) As precision agriculture
431 management decisions are normally based on imagery, soil and climate conditions, AirSurf's results
432 will be more reliable, if we could include soil conditions for each harvest region and field-level climate
433 conditions. So, results can be compared between sites in multiple years. A potential approach is to
434 incorporate ground-based phenotyping systems such as CropSight⁴⁵ to feed environment information
435 to the analysis. (4) The method was tested and validated in lettuce fields in a number of geographic

436 locations following a standard aerial imaging procedure, data collected from different sites via varied
437 aerial imaging strategies (e.g. different angles, altitudes and GSD) could improve the soundness and
438 compatibility of the platform. (5) Key features were constructed by learning algorithms instead of
439 engineered, which make learning models vulnerable when facing up to totally undefined datasets.
440 Hence, ML/DL based phenotypic analysis algorithms need to update with new labelled training data in
441 order to avoid training issues encountered by us. (6) For a field of approximately one million lettuces,
442 it takes about four hours to analyse a field on a decent computer (2.5GHz Intel Core i7, 8 GB memory).
443 Most of the computational time is occupied by the learning model to identify individual lettuces, which
444 can be improved by parallel computing or GPU (graphic processing unit) processing to speed up the
445 phenotypic analysis.

446

447 *Prospects for crop research and precision agriculture*

448 Together with recent advances in multi-scale remote sensing and phenotyping data management⁴⁵⁻⁴⁷,
449 the platform could be relatively easily expanded to incorporate other crop species such as wheat and
450 rice by retraining the learning models with additional datasets. By doing so, AirSurf could be developed
451 into a more comprehensive analytic platform that will bring great significance to crop production,
452 marketable yield, and precision agriculture management for the Agri-Food sector. For example, the
453 plant density of wheat and rice is closely related to the yield due to its influences on the allocation of
454 water, light and fertilisers, which cannot be quantified using ground-based RGB imagery⁴⁸. Hence,
455 utilising the ultra-scale NDVI aerial imagery and related object recognition methods embedded in
456 AirSurf-L, it is likely to benefit the assessment of sowing performance, emergence rate, and plant
457 distribution. Through a multi-scale field phenotyping approach, breeders and crop researchers could
458 make early predictions of the grain yield of crop genotypes in field experiments.

459 From a precision agriculture perspective, monitoring individual plant such as a lettuce head can enable
460 accurate monitoring of crops during key growth stages across a plantation site. It can provide growers
461 with the real number of crops in the field, based on which yield for harvest availability can be quantified
462 instead of estimated. The calculation of in-field crops can also lead to accurate agricultural inputs,

463 facilitating automated variable-rate application of fertiliser, weed control, and pesticides through tractor
464 software system with a more precise crop distribution map⁴⁹. Furthermore, the close monitoring of key
465 yield-related traits can be used to guide farmers and growers to reduce variability of agrichemical
466 applications and irrigation in different fields, increasing harvest yield and better operating profit
467 margin⁵⁰. Finally, the AirSurf-L platform utilises existing aerial imagery data routinely performed by
468 growers, which means that no extra data collection cost is required, which is an important factor for
469 new Agri-Tech solutions to be adopted by the Agri-Food sector.

470

471 **Conclusions**

472 AirSurf-Lettuce automatically measures infield iceberg lettuces using ultra-scale NDVI aerial images,
473 with a focus on yield-related traits such as lettuce number, size categories, field size distribution, and
474 GPS-tagged harvest regions. The analysis results are close to the manual counting and can be used to
475 improve existing in-field crop estimates. By monitoring millions of lettuces in the field, we demonstrate
476 the significant value of AirSurf-L in ultra-scale field phenotyping, precise harvest strategies, and crop
477 marketability before the harvest. We believe that our algorithm design, software implementation, the
478 application of ML/DL and CV algorithms, and the cross-disciplinary R&D will be highly valuable for
479 future plant phenomics research that are destined to be more and more challenging. With continuous
480 development work, we are confident that the platform has great potential to support the Agri-Food
481 sector with a smart and precise crop surveillance approach of vegetable crops and therefore lead to
482 better precision agriculture management decisions.

483

484 **Availability and requirements**

485 Project name: AirSurf-Lettuce with G's Growers

486 Project home page: <https://github.com/Crop-Phenomics-Group/Airsurf-Lettuce>

487 Source code: <https://github.com/Crop-Phenomics-Group/AirSurf-Lettuce/>

488 GUI software: <https://github.com/Crop-Phenomics-Group/AirSurf-Lettuce/releases>

489 Operating system(s): platform independent

490 Programming language: Python 3.6
491 Requirements: Keras, TensorFlow, Skimage, and Numpy.
492 License: BSD-3-Clause available at <https://opensource.org/licenses/BSD-3-Clause>

493

494 **Abbreviations**

495 Comma-separated values (CSV), computer vision (CV), convolutional neural networks (CNNs), deep
496 learning (DL), global positioning system (GPS), ground sample distance (GSD), machine learning (ML),
497 non-maximum suppression algorithm (NMS), normalized difference vegetation index (NDVI), rectified
498 linear units (ReLU), the United Kingdom (UK), and Unmanned Aerial Vehicles (UAVs).

499

500 **Availability of supporting data**

501 The datasets supporting the results presented here is available at [https://github.com/Crop-Phenomics-](https://github.com/Crop-Phenomics-Group/Airsurf-Lettuce/releases)
502 [Group/Airsurf-Lettuce/releases](https://github.com/Crop-Phenomics-Group/Airsurf-Lettuce/releases). Source code and other supporting data are also openly available in the
503 GitHub repository.

504

505 **Author contributions**

506 J.Z., A.G.B., A.B. and J.K. wrote the manuscript, S.M.R. performed the NDVI imaging. J.K. and S.M.R.
507 provided harvest information and biological expertise. J.Z., A.G.B., and C.A. designed the analysis
508 algorithms. A.B., A.G.B., C.A. and J.Z. implemented the software solution. A.G.B. and A.B. built the
509 deep learning models. J.B. packaged the GUI executables. J.Z., A.B., A.G.B., C.A., S.L. and J.B. tested
510 the software and performed the data analysis. All authors read and approved the final manuscript.

511

512 **Funding**

513 J.Z. was partially funded by UKRI Biotechnology and Biological Sciences Research Council's (BBSRC)
514 Designing Future Wheat Cross-institute Strategic Programme (BB/P016855/1) to Graham Moore,
515 BBS/E/T/000PR9785 to J.Z.; J.B. were partially supported by the Core Strategic Programme Grant
516 (BB/CSP17270/1) at the Earlham Institute; A.G.B. and C.A. were also partially supported by G's

517 Growers's industrial fund awarded to J.Z.; A.B. was partially supported by the Newton UK-China Agri-
518 Tech Network+ Grant (GP131JZ1G) awarded to J.Z.

519

520 **Acknowledgements**

521 The authors would like to thank all members of the Zhou laboratory at EI and Nanjing Agricultural
522 University for fruitful discussions and cross-country collaborations. We thank researchers at John Innes
523 Centre and UEA for constructive suggestions. We gratefully acknowledge the support of NVIDIA
524 Corporation with the award of the Quadro GPU used for this research.

525

526 **Competing interests**

527 The authors declare no competing financial interests.

528

529 **References**

- 530 1 Gubbi J, Buyya R, Marusic S, Palaniswami M. Internet of Things (IoT): A Vision, Architectural
531 Elements, and Future Directions. *Futur Gener Comput Syst* 2013; **29**: 1645–1660.
- 532 2 Mou B. Mutations in lettuce improvement. *Int J Plant Genomics* 2011; **2011**: 1–7.
- 533 3 Koudela M, Petříková K. Nutrients content and yield in selected cultivars of leaf lettuce (*Lactuca sativa*
534 *L. var crispa*). *Hortic Sci* 2008; **35**: 99–106.
- 535 4 Tei F, Scaife A, Aikman D. Growth of lettuce, onion, and red beet. 1. Growth analysis, light
536 interception, and radiation use efficiency. *Ann Bot* 1996; **78**: 633–643.
- 537 5 BBC. Iceberg lettuces and broccoli rationed as vegetable crisis hits supermarkets. BBC News. 2017; :
538 1–3.
- 539 6 Jie H, Lee Sing Kong. Growth and photosynthetic characteristics of lettuce (*Lactuca sativa* L.) under
540 fluctuating hot ambient temperatures with the manipulation of cool root-zone temperature. *J Plant*
541 *Physiol* 1998; **152**: 387–391.
- 542 7 Johkan M, Shoji K, Goto F, Hashida S nosuke, Yoshihara T. Blue light-emitting diode light irradiation
543 of seedlings improves seedling quality and growth after transplanting in red leaf lettuce. *HortScience*
544 2010; **45**: 1809–1814.

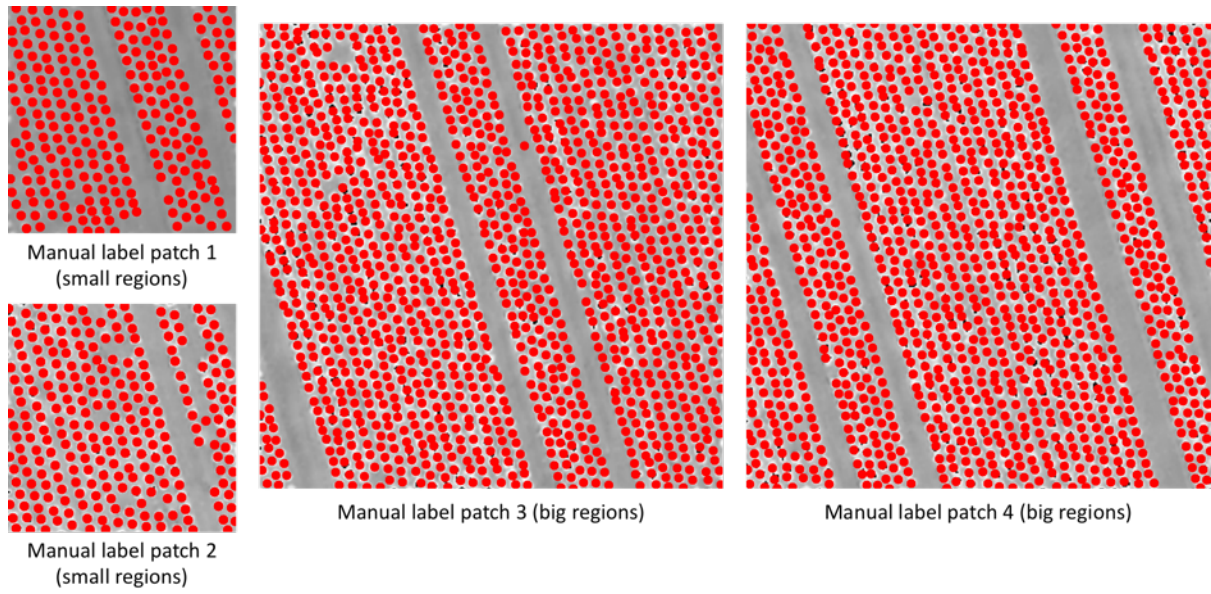
- 545 8 Ogbodo EN, Okorie PO, Utobo EB. Growth and Yield of Lettuce (*Lactuca sativa* L.) At Abakaliki
546 Agro-Ecological Zone of Southeastern Nigeria. *World J Agric Sci* 2010; **6**: 141–148.
- 547 9 Tudela JA, Hernández N, Pérez-Vicente A, Gil MI. Growing season climates affect quality of fresh-cut
548 lettuce. *Postharvest Biol Technol* 2017; **123**: 60–68.
- 549 10 Sankaran S, Khot LR, Espinoza CZ *et al.* Low-altitude, high-resolution aerial imaging systems for row
550 and field crop phenotyping: A review. *Eur J Agron* 2015; **70**: 112–123.
- 551 11 Duan T, Zheng B, Guo W *et al.* Comparison of ground cover estimates from experiment plots in cotton,
552 sorghum and sugarcane based on images and ortho-mosaics captured by UAV. *Funct Plant Biol* 2016.
553 doi:10.1071/FP16123.
- 554 12 Meyer GE, Neto JC. Verification of color vegetation indices for automated crop imaging applications.
555 *Comput Electron Agric* 2008; **63**: 282–293.
- 556 13 Yang G, Yang X, Zhang X *et al.* Unmanned Aerial Vehicle Remote Sensing for Field-Based Crop
557 Phenotyping: Current Status and Perspectives. *Front Plant Sci* 2017; **8**: 1–27.
- 558 14 Rousseau D, Dee H, Pridmore T. Imaging Methods for Phenotyping of Plant Traits. In: Kumar S (ed).
559 *Phenomics in Crop Plants: Trends, Options and Limitations*. Springer India, 2015, pp 61–74.
- 560 15 Tsafaris SA, Minervini M, Scharr H. Machine Learning for Plant Phenotyping Needs Image
561 Processing. *Trends Plant Sci* 2016; **21**: 989–991.
- 562 16 Burrige J, Jochua CN, Bucksch A, Lynch JP. Legume shovelomics: High-Throughput phenotyping of
563 common bean (*Phaseolus vulgaris* L.) and cowpea (*Vigna unguiculata* subsp. *unguiculata*) root
564 architecture in the field. *F Crop Res* 2016; **192**: 21–32.
- 565 17 Bradley D, Xu P, Mohorianu I-I *et al.* Evolution of flower color pattern through selection on regulatory
566 small RNAs. *Science (80-)* 2017; **358**: 925–928.
- 567 18 Angermueller C, Pärnamaa T, Parts L, Stegle O. Deep learning for computational biology. *Mol Syst Biol*
568 2016; **12**: 878.
- 569 19 Großkinsky DK, Pieruschka R, Svendsgaard J *et al.* Phenotyping in the fields: Dissecting the genetics of
570 quantitative traits and digital farming. *New Phytol* 2015; **207**: 950–952.
- 571 20 Zaman-Allah M, Vergara O, Araus JL *et al.* Unmanned aerial platform-based multi-spectral imaging for
572 field phenotyping of maize. *Plant Methods* 2015; **11**: 35.
- 573 21 Simms DM, Waine TW, Taylor JC, Juniper GR. The application of time-series MODIS NDVI profiles
574 for the acquisition of crop information across Afghanistan. *Int J Remote Sens* 2014; **35**: 6234–6254.

- 575 22 Pound MP, Atkinson JA, Townsend AJ *et al.* Deep machine learning provides state-of-the-art
576 performance in image-based plant phenotyping. *Gigascience* 2017; **6**: 1–10.
- 577 23 Rosebrock A. *Deep Learning for Computer Vision with Python*. 2017
578 doi:10.1017/CBO9781107415324.004.
- 579 24 Reza AM. Realization of the contrast limited adaptive histogram equalization (CLAHE) for real-time
580 image enhancement. *J VLSI Signal Process Syst Signal Image Video Technol* 2004; **38**: 35–44.
- 581 25 Shipman JW. Tkinter 8.5 reference: a GUI for Python. New Mexico,
582 2013<http://www.nmt.edu/tcc/help/pubs/tkinter/>.
- 583 26 Zhou J, Applegate C, Alonso AD *et al.* Leaf-GP: An open and automated software application for
584 measuring growth phenotypes for arabidopsis and wheat. *Plant Methods* 2017; **13**: 1–31.
- 585 27 Alex K, Ilya S, Geoffrey EH. ImageNet Classification with Deep Convolutional Neural Networks. In:
586 *Neural information processing systems*. Neural Information Processing Systems (NIPS): Lake Tahoe,
587 Nevada, 2012, pp 1097–1105.
- 588 28 Choromanska A, Henaff M, Mathieu M, Arous G Ben, LeCun Y. The Loss Surface of Multilayer
589 Networks. *arXiv14120233 [cs]* 2014.
- 590 29 Matsugu M, Mori K, Mitari Y, Kaneda Y. Subject independent facial expression recognition with robust
591 face detection using a convolutional neural network. *Neural Networks* 2003; **16**: 555–559.
- 592 30 Neubeck A, Van Gool L. Efficient non-maximum suppression. *Proc - Int Conf Pattern Recognit* 2006;
593 **3**: 850–855.
- 594 31 Hazan E. Introduction to Online Convex Optimization. *Found Trends Optim* 2015; **2**: 151–166.
- 595 32 Hunter JD. Matplotlib: A 2D Graphics Environment. *Comput Sci Eng* 2007; **9**: 90–95.
- 596 33 Furbank RT, Tester M, Berry S *et al.* Phenomics – technologies to relieve the phenotyping bottleneck.
597 *Trends Plant Sci* 2011; **16**: 635–644.
- 598 34 Tardieu F, Cabrera-Bosquet L, Pridmore T, Bennett M. Plant Phenomics, From Sensors to Knowledge.
599 *Curr Biol* 2017; **27**: R770–R783.
- 600 35 ZHOU J, Tardieu F, Pridmore T *et al.* Plant phenomics: history, present status and challenges. *J Nanjing*
601 *Agric Univ* 2018; **41**: 580–588.
- 602 36 Cendrero-Mateo MP, Muller O, Albrecht H *et al.* Field Phenotyping: Challenges and Opportunities.
603 *Terr Ecosyst Res Infrastructures* 2017; : 53–80.
- 604 37 Galinato SP, Miles CA. Economic profitability of growing lettuce and tomato in western washington

- 605 under high tunnel and open-field production systems. *Horttechnology* 2013; **23**: 453–461.
- 606 38 Mulderij R. OVERVIEW GLOBAL LETTUCE MARKET. Tholen,
607 2016<http://www.freshplaza.com/article/163938/OVERVIEW-GLOBAL-LETTUCE-MARKET>.
- 608 39 Shukla M, Jharkharia S. *Agri-fresh produce supply chain management: A state-of-the-art literature*
609 *review*. 2013 doi:10.1108/01443571311295608.
- 610 40 Lamsal K, Jones PC, Thomas BW. Harvest logistics in agricultural systems with multiple, independent
611 producers and no on-farm storage. *Comput Ind Eng* 2016; **91**: 129–138.
- 612 41 Schiefer G. New technologies and their impact on the agri-food sector: An economists view. *Comput*
613 *Electron Agric* 2004; **43**: 163–172.
- 614 42 Singh A, Ganapathysubramanian B, Singh AK, Sarkar S. Machine Learning for High-Throughput Stress
615 Phenotyping in Plants. *Trends Plant Sci* 2016; **21**: 110–124.
- 616 43 Pedregosa F, Varoquaux G, Gramfort A *et al*. Scikit-learn: Machine Learning in Python. *J Mach Learn*
617 *Res* 2011; **12**: 2825–2830.
- 618 44 van der Walt S, Schönberger JL, Nunez-Iglesias J *et al*. Scikit-image: image processing in Python.
619 *PeerJ* 2014; **2**: 1–18.
- 620 45 Reynolds D, Ball J, Bauer A *et al*. CropSight : a scalable and open-source information management
621 system for distributed plant phenotyping and IoT-based crop management. *Gigascience* 2019; **8**: 1–35.
- 622 46 Reynolds D, Baret F, Welcker C *et al*. What is cost-efficient phenotyping? Optimizing costs for
623 different scenarios. *Plant Sci* 2018; **July**. doi:10.1016/j.plantsci.2018.06.015.
- 624 47 Neveu P, Tireau A, Hilgert N *et al*. Methods Dealing with multi-source and multi-scale information in
625 plant phenomics : the ontology-driven Phenotyping Hybrid Information System. *New Phytol* 2018; **221**:
626 588–601.
- 627 48 Liu S, Baret F, Andrieu B, Burger P, Hemmerlé M. Estimation of Wheat Plant Density at Early Stages
628 Using High Resolution Imagery. *Front Plant Sci* 2017; **8**: 1–10.
- 629 49 Frasconi C, Raffaelli M, Emmi L, Fontanelli M, Martelloni L, Peruzzi A. An automatic machine able to
630 perform variable rate application of flame weeding: Design and assembly. *Chem Eng Trans* 2017; **58**:
631 301–306.
- 632 50 Brann D, Specialist EG, Sciences SE, Tech V. A Comprehensive Approach Precision Farming :
633 Management is the KEY. *Virginia Coop Ext* 2009.
- 634

635 **Supplementary Figures**

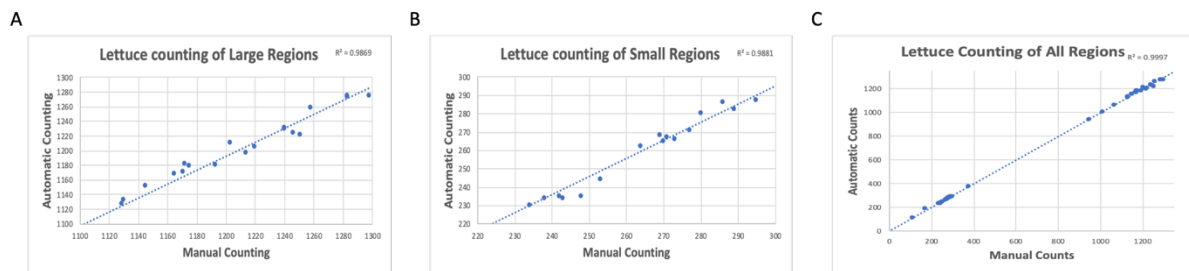
636 **Supplementary Figure 1: Manually labelled lettuces in randomly selected patches using red dots.**



637

638

639 **Supplementary Figure 2: The correlation between human counting and AirSurf-L scoring.**



640

641